



OPEN ACCESS

EDITED BY

Marco Fontana,
Polytechnic University of Turin, Italy

REVIEWED BY

Gianluca Milano,
National Institute of Metrological Research
(INRiM), Italy
Federico Raffone,
Polytechnic University of Turin, Italy

*CORRESPONDENCE

Davide Cipollini,
✉ d.cipollini@rug.nl
Francesca Borghi,
✉ francesca.borghi@unimi.it

†These authors share first authorship

RECEIVED 13 February 2024

ACCEPTED 20 May 2024

PUBLISHED 07 June 2024

CITATION

Cipollini D, Profumo F, Schomaker L, Milani P
and Borghi F (2024), Conduction mechanisms
in a planar nanocomposite resistive switching
device based on cluster-assembled Au/ZrO_x
films.

Front. Mater. 11:1385792.

doi: 10.3389/fmats.2024.1385792

COPYRIGHT

© 2024 Cipollini, Profumo, Schomaker, Milani
and Borghi. This is an open-access article
distributed under the terms of the [Creative
Commons Attribution License \(CC BY\)](#). The
use, distribution or reproduction in other
forums is permitted, provided the original
author(s) and the copyright owner(s) are
credited and that the original publication in
this journal is cited, in accordance with
accepted academic practice. No use,
distribution or reproduction is permitted
which does not comply with these terms.

Conduction mechanisms in a planar nanocomposite resistive switching device based on cluster-assembled Au/ZrO_x films

Davide Cipollini^{1,2*†}, Filippo Profumo^{3†}, Lambert Schomaker^{1,2},
Paolo Milani³ and Francesca Borghi^{3*}

¹Bernoulli Institute for Mathematics, Computer Science and Artificial Intelligence, University of Groningen, Groningen, Netherlands, ²CogniGron—Groningen Cognitive Systems and Materials Center, Groningen, Netherlands, ³CIMAINA—Interdisciplinary Centre for Nanostructured Materials and Interfaces, Department of Physics “Aldo Pontremoli”, University of Milan, Milano, Italy

Nanostructured zirconia and gold films (ns-Au/ZrO_x) have been demonstrated as devices characterized by non-linear and hysteretic electrical behavior, with short-term memory and potentiation/depression activity. Here we investigate the conduction mechanisms regulating the non-linear behavior of the nanostructured bilayer Au/ZrO_x films. In particular, we investigated the hysteretic I-V curves following the Chua's approach to memristive systems and separately modelling ion migration and electron transport in the films. The conduction mechanisms exhibited by the bilayered nanostructured system are strongly influenced by the nanogranular morphology that dynamically changes because of electrical stimuli; structural rearrangements are particularly promoted by intense local electric fields and high mobility along bottlenecks and edges in the microstructure. Electron transport is accounted for the Schottky barrier at the electrode interfaces and Poole-Frenkel effect in the bulk nanogranular material, according to a dynamic reorganization of the cluster-assembled network. A model for Poole-Frenkel effect is here discussed to include saturation of the Coulombic traps in the high applied field regime; the proposed model has been validated with experimental voltage ramps with varying sweep-velocity and at different temperatures (from 300 to 200 K), as also by a power exponent parameter analysis.

KEYWORDS

neuromorphic device, resistive switching, nanostructured films, Poole-Frenkel conduction, Schottky interface

1 Introduction

A memristor is a two-port passive electronic element whose conductance depends on the history of the applied signal (Chua, 1971). According to the formal description given by (Chua and Kang, 1976), a flux-controlled memristor is a device governed by the two following equations:

$$\frac{dw}{dt} = f(w, v) \quad (1)$$

$$i(t) = G(w, v)v(t) \quad (2)$$

where w is the state variable, v is the voltage applied and i is the output current.

After the fabrication of a nanoscale physical memristor by (Strukov et al., 2008), memristive devices have gained increasing attention as they have shown potential predisposition for neuromorphic applications (Mead, 2020) and low power signal processing devices (Christensen et al., 2022). Their synaptic-like behavior is of practical relevance for the emulation of brain computational and learning capabilities in spiking neural networks (Indiveri et al., 2013), as well as to build crossbar arrays for energy efficient hardware for computing steps in artificial intelligence algorithms (Wang et al., 2019; Xia and Yang, 2019).

In literature, memristive systems are most often composed by an insulator thin layer sandwiched between two metal electrodes. To describe the electrical behavior of these devices multiple models are available in the literature, e.g., (Pickett et al., 2009; Laiho et al., 2010; Chang et al., 2011; Yakopcic et al., 2013). We refer to (Linn et al., 2014) for an exhaustive discussion on the applicability of well-established memristive models to describe the complex nonlinear dynamical behavior of such devices.

Fabrication of planar memristors has also been reported. Even though these systems are less represented in the literature, they offer unique opportunities for complex signal information processing applications and for interfaces with biological systems (Fu et al., 2020; Liu et al., 2020). In fact, the planar geometry allows the multi-electrode set up which is a major deviation from the classical two-terminal device paradigm. Thus, a bottom-up self-assembled memristive network connects the electrodes without any top-down construction required for crossbar arrays. In other words, the electrodes take the role of “neurons” while the substrate takes the role of the recurrent synaptic network connecting the neurons. Moreover, these systems allow a larger number of resistance values than a single memristor and increased tunability of the voltage threshold as consequence of the choice of the input/output electrode configuration in the network.

They also provide hardware substrates for application of computing paradigms involving highly dimensional dynamical systems, e.g., reservoir computing (Jaeger, 2001) or echo state networks (Maass et al., 2002), and the collective properties of associative memory, e.g., in Hopfield networks (Hopfield, 1982) and Boltzmann machines (Hinton and Brown, 1999). In the high-dimensional computing paradigm, a key role is played by the large number of elements involved in the computation, enabling higher resistance to noise and fault-tolerant computation capabilities similar to what happens in the brain.

Among a large number of metal oxides used for memristor fabrication, ZrO_2 received considerable attention owing to its belonging to high- k dielectrics with high permittivity, simple composition, easy fabrication, and its compatibility with standard CMOS fabrication processes (Sun et al., 2009; Parreira et al., 2016). Recently, sandwiched devices with yttria-stabilized zirconia (YSZ) active layers, exhibiting bipolar resistive switching, have been proposed and regarded as filamentary switching (Gorshkov et al., 2016). They utilized Conductive Atomic Force Microscopy (CAFM) to induce single filament formation in thin YSZ layers, also exploiting Au islands in an underlying layer (Filatov et al., 2017), or Au NPs (Filatov et al., 2018) to concentrate the electric field. Other studies developed a model for device behavior based on oxygen

vacancies redistribution (Guseinov et al., 2017). Further electrical characterization techniques revealed insights into ions migration and resistive switching activity (Tikhov et al., 2018; Ryabova et al., 2022), while also demonstrating multi-level device capabilities and neuromorphic behavior akin to Spike Timing-Dependent Plasticity (STDP) (Emelyanov et al., 2019).

In alternative to top-down fabrication approaches, bottom-up self-assembling of nano-objects such as nanowires, nanoparticles and domain walls is gaining increasing attention for the fabrication of neuromorphic devices for different applications (Bose et al., 2017; Mirigliano and Milani, 2021; Zhu et al., 2021; Milano et al., 2022; Rieck et al., 2023; Cipollini et al., 2024). Recently a planar resistive switching system based on nanostructured Au/ZrO_x showing short-term plasticity and with structural characteristics compatible with the conditions of *in vitro* cell culture has been reported (Profumo et al., 2023). The system consists of the superposition of two layers: the bottom one made of a cluster-assembled gold film and the top one of a cluster-assembled zirconia film. Nanostructured zirconia films have interesting biocompatible properties (Schulte et al., 2016; 2018; Previdi et al., 2023) which make them suitable as biological/artificial interface. The non-ohmic and resistive switching behavior of gold cluster-assembled films (CAFs), due to the reorganization of grain boundaries and defects at the interfaces of the nanogranular films (Casu et al., 2024), has been reported also in (Mirigliano et al., 2019; Nadalini et al., 2023); by coupling gold with zirconia CAFs, it is possible to obtain a system exhibiting additional neuromorphic properties such as short-time retention (order of seconds) with stretched-exponential relaxation, and potentiation/depotentiation (Profumo et al., 2023).

Here we investigate the conduction mechanisms of the bilayered nanostructured Au/ZrO_x films and we propose a memristive-like model to describe the hysteresis properties of this system: given the large size of the device (4 mm conductive path length) and the large dynamical range of voltage input signal, previously mentioned models for memristors are not able to outline the physical conduction mechanisms since bulk conduction has an important role in this case. We thus develop a model that integrates an ideal bulk-limited and electrode-limited conduction mechanisms. The former addresses conduction in the low resistance state by a modern model of Poole-Frenkel (PF) effect, promoted by the grain boundaries and granularity of the material (Felix et al., 2011). Electrode limited conduction by the Schottky effect is used for the high-resistance state. Finally, an analysis of the power exponent parameter $G = d \ln(I) / d \ln(V)$ (Acha, 2017) is discussed and an experimental characterization of the electrical response of the bilayered film at different temperatures supports the model proposed.

2 Materials and methods

2.1 Nanostructure fabrication

Ns- Au/ZrO_x bilayer films are deposited on a commercial glass coverslip (Zeus 2 cm × 2 cm × 1 mm) cleaned in an ethanol ultrasonic bath for 15 min. The two gold electrodes have been deposited by thermal evaporation and they are separated by a 4 mm long gap. Electrode's dimensions are 3 mm × 7 mm × 80 nm. A

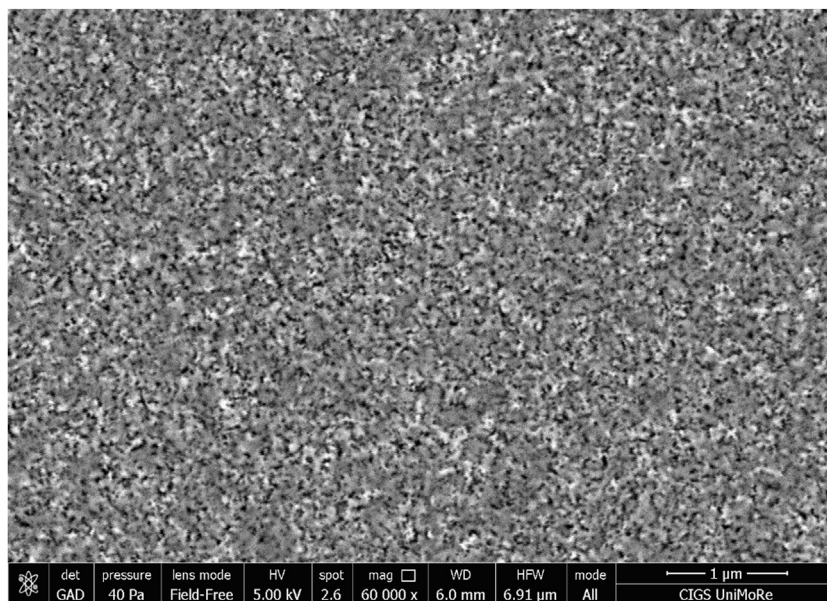


FIGURE 1
ESEM (ESEM Quanta 200) image of the granular structure of the ns-Au/ZrO_x nanocomposite.

30 nm thick gold nanostructured film (ns-Au) is deposited using a Supersonic Cluster Beam Deposition (SCBD) apparatus (Milani and Iannotta, 1999; Borghi et al., 2022), filling the gap between the two electrodes with a strip 1 mm large and 6 mm long. Subsequently, a zirconia (ZrO_x) nanostructured film of 90 nm thickness is deposited with the same aforementioned apparatus, on the top of the gold thin film (Borghi et al., 2018). The SCBD apparatus is equipped with a Pulsed Microplasma Cluster Source (PMCS) that allows the production of neutral clusters in the gas phase, as described in detail in (Wegner et al., 2006). For further details about fabrication method, we refer to our previously published paper (Profumo et al., 2023). In Figure 1, an Environmental Scanning Electron Microscopy (ESEM) image of the nanocomposite is displayed, showing the granular and porous structure of the ns-Au/ZrO_x thin film.

2.2 Electrical measurement

The as-deposited layered ns-Au/ZrO_x films shows ohmic electrical behavior as previously reported for the single layer of ns-Au film (Mirigliano et al., 2019). After the application of constant voltage higher than roughly 16 V, the device switches to the high resistance state ascribed to the partial breaking and reorganization of the underlying ns-Au film, a so-called forming process, well described for ns-Au film in (Nadalini et al., 2023). Figure 2 shows representative snapshots of the electrical response during the forming process of the non-linear electrical behavior of the bilayered samples: this process is related to a joule heating effect at low voltages A), a non-trivial reorganization of the network at higher voltages due to both heating effects and electroforming mechanisms B) and an abrupt increase in sample resistance at a critical voltage C).

After the forming process, the device shows a non-linear and hysteretic behavior reported in Figure 3. I-V curves are obtained

applying DC voltages starting from -20 V to $+20$ V with velocity sweep 1V/s and 2.3V/s. The measurements show that for faster voltage sweeps higher currents are obtained. We observe peculiar electrical behaviors consisting in the opening of the curves at non-zero voltage and non-zero current and a saturation effect almost independent of the velocity of the voltage sweep. As first approximation, we discuss in the next Section 2.4 the saturation effect that is ascribable to the saturation of the PF conduction mechanism at a certain critical applied field.

We verified the stability of the IV curves acquired at the different sweep velocities for ten cycles, as it is reported in Supplementary Material (Supplementary Figure S1). Furthermore, we evaluated the variability of the conduction responses for different devices, nominally identical, i.e., with the same ns-Au and ns- ZrO_x thicknesses. In the Supplementary Material (Supplementary Figure S2) the box plots of the main electrical parameters of eight devices (initial resistance before the forming process, resistance after forming process, current value at 20 V and maximum percentual difference between forward and backward currents at fixed voltage) are reported. We noticed the same hysteretic and non-linear behavior, with the highest variability in the current values, principally due to low reproducibility of the contact area between the bilayered nanogranular structure and the bulk electrodes, which affects the current flowing in the devices.

2.3 Electrical measurements at variable temperature

In situ electrical characterization with temperature spanning from ambient temperature (300 K) to 200 K, has been performed in vacuum ($p < 10^{-4}$ mbar) on films mounted on a copper cold finger of a helium mechanical cryocooler. I-V measurements are performed

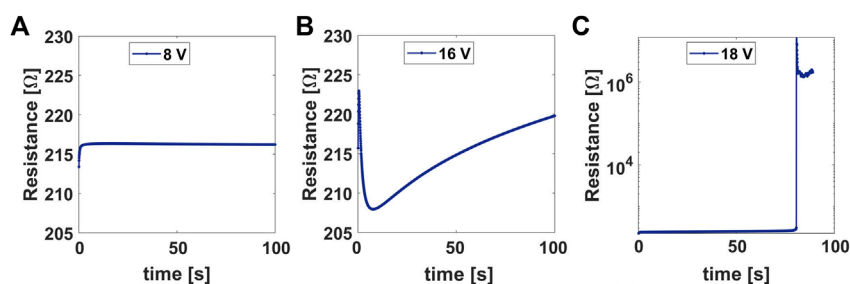


FIGURE 2

Snapshots of the forming process of the non-linear electrical behavior in bilayered nanostructured sample. (A) Resistance in time at constant voltage 8 V showing initial joule heating effect, (B) resistance at 16 V showing an electrical response driven by the reorganization of the network, (C) resistance at 18 V with an abrupt increase as indicator of an irreversible reorganization of the network.

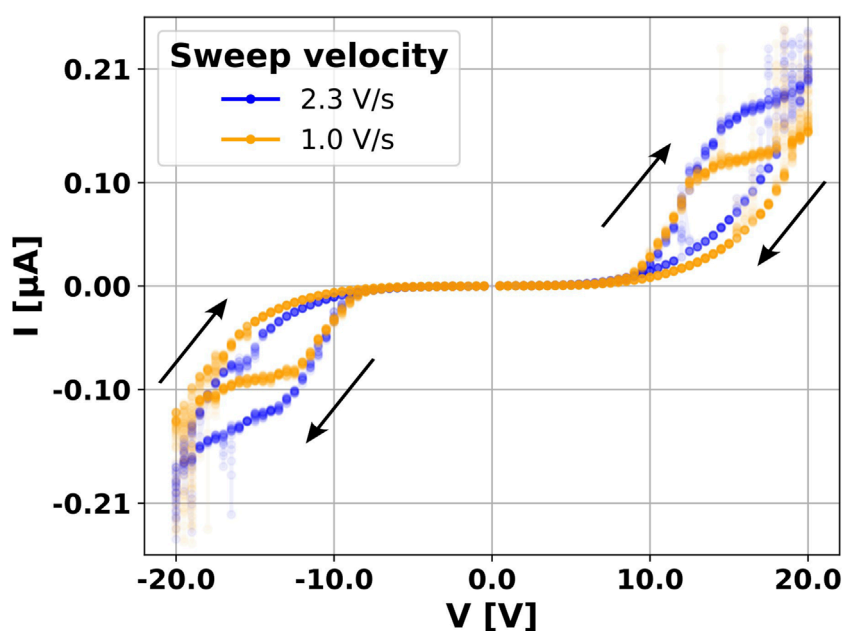


FIGURE 3

DC I-V sweep for layered Au/ZrO_x sample after resistive switching activation. Legend shows voltage sweep velocities. Arrows illustrate the curve path direction.

with a SPD3303X-E Programmable DC Power Supply and an Agilent 34410A multimeter at 2V/s and 1V/s.

2.4 Saturation of the Poole-Frenkel effect

Before describing the memristive-like model developed for our device, we discuss the Poole-Frenkel (PF) effect both in the classical formulation (Frenkel, 1938) and in the modern formulation (Ongaro and Pillonnet, 1989), which incorporates a saturation effect that must be included in a complete model for an emptying-trap process.

The PF effect can be illustrated (see Figure 4A) as the reduction of the potential barrier trapping the electrons to the Coulombic (charged) centers in the bulk material as a consequence of the applied electric field. Consequently, the escape probability of

electrons by thermal excitation is increased by the application of the field. In Figure 4A curve a) shows the typical Coulombic potential as a function of the distance from the charged trap. As the electric field is applied, the electron needs smaller energy to escape the attraction of the trap which is reduced by an amount equal to $\beta\sqrt{E}$. Once the electron gains the necessary ionisation energy by thermal excitation, it is promoted to the conduction band, or the quasi-conduction band in the case of amorphous materials (Hill, 1971). Thus, there exists a critical value of the applied field such that the potential wall is reduced to the ground state of the trap (see curve c) in Figure 4A). In such a case, no barrier is present and the charged donor traps are completely ionised, thus a saturation effect must be taken into account when high fields are involved.

In the classical formulation (Frenkel, 1938), and in its variations available in the literature, the conductivity σ of the bulk material is

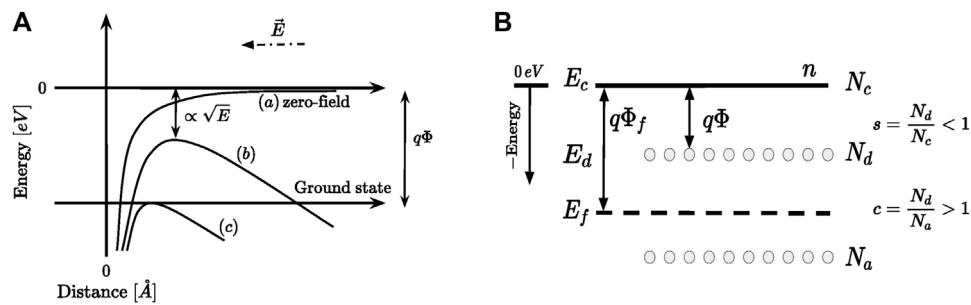


FIGURE 4

(A) Schematic illustration of the PF effect. The electric field (dashed arrow) lowers the Coulombic potential well. If no field is applied an ionization energy equal to $q\Phi$ is required (see curve (a)). Curve (b) illustrates the case of a non-zero electric field applied. Curve (c) shows the saturation effect: for a sufficiently large electric field applied, there is no effective barrier trapping the electron, thus the donor trap centers are ionized. Only the right side of the potential well is depicted. (B) Representative band diagram illustrating the PF effect as described in the original work. The energy levels of the conduction band, E_c , the donor level, E_d , and the Fermi level E_f are depicted. The relative position of E_d and E_f is arbitrary. N_d and N_a indicate the density of donor traps and acceptors. Both panels (A) and (B) are adapted from (Ongaro and Pillonnet, 1989; Harrell and Gopalakrishnan, 2002).

proportional to:

$$\sigma \propto e^{-\frac{(q\Phi - \beta\sqrt{E})}{KT}} \propto e^{\alpha\sqrt{E}} \quad (3)$$

where E is the external applied field, K is the Boltzmann constant, T is the temperature, $q\Phi$ is the ionisation potential and $\beta = \sqrt{q^3/\pi\epsilon\epsilon_0}$ is the PF constant, where q is the charge of the electron and ϵ and ϵ_0 are the dielectric constants of the vacuum and of the amorphous material respectively.

Thus, the current density J is proportional to:

$$J \propto \sigma E \propto E e^{\alpha\sqrt{E}} \quad (4)$$

As firstly recognized in (Ongaro and Pillonnet, 1989), the conductivity, σ , in equation 3 is an indefinitely increasing function of the applied field, which is in obvious contrast with the emptying of the donor traps underlying the PF effect described above. This inconsistency is due to the use of the Boltzmann function as a steadily adopted and convenient approximation of the Fermi-Dirac in the literature. Specifically, Ongaro and Pillonnet demonstrated that the use of the Fermi-Dirac function to describe the population statistics of the donor traps in their model leads to the description of the saturation of the PF effect at high fields. We report here their assumptions (Ongaro and Pillonnet, 1989; Harrell and Gopalakrishnan, 2002) which we consider valid to model our device in the following:

- The acceptor levels are positioned well-below the Fermi level (see Figure 4B) thus they are completely filled for all values of field and temperature.
- It exists a single donor level at depth Φ below the conduction band, i.e., $q\Phi$ is the ionization energy.
- The density of donor traps is greater than the acceptor density, i.e., $c = N_d/N_a > 1$. The ionized donors and the acceptors are assumed to lie apart disabling any interaction between the two, even though for values of $c \rightarrow 1$ and large N_d values the assumption is difficult to maintain. The ratio between the donor density and the density of states at the bottom of the conduction band is $s = N_d/N_c < 1$.

- The Boltzmann function is used only to describe the statistics of the electrons populating the bottom of the conduction band, $n = N_c \exp((E_c - E_f)/KT)$.
- The Fermi-Dirac function evaluated at the donor energy level describes the probability of occupancy of electrons in the trap's sites:

$$f(E_d) = \frac{1}{1 + e^{(E_d - E_f)/KT}} \quad (5)$$

The use of the Fermi-Dirac permits the description of the saturation and permits to avoid assumptions on the relative position of the energy levels of E_d and E_f , as in previous models.

Thanks to the assumption that all acceptors are filled, the equation of conservancy of the charge can be written in the form of $n_d = n + N_a$, which leads to the expression of the relative density of electrons in the conduction band $n_r = n/N_c$:

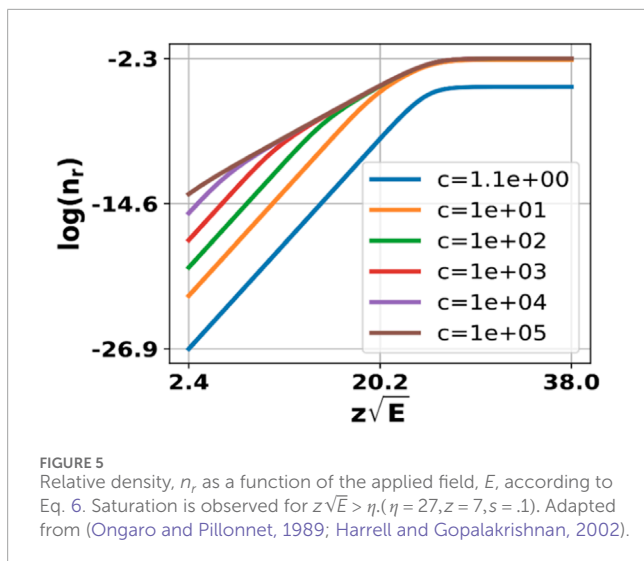
$$n_r = \frac{n}{N_c} = \frac{1}{2} e^{-\eta + z\sqrt{E}} \left(1 + \frac{s}{c} e^{\eta - z\sqrt{E}} \right) \cdot \left(\sqrt{1 + \frac{4s(c-1)e^{\eta - z\sqrt{E}}}{c \left(1 + \frac{s}{c} e^{\eta - z\sqrt{E}} \right)^2}} - 1 \right) \quad (6)$$

where $\eta = q\Phi/KT$ and $z = \beta/KT$. For the detailed derivation of the above equation, we refer to the original paper (Ongaro and Pillonnet, 1989) and to the more recent paper (Harrell and Gopalakrishnan, 2002). Figure 5 shows the saturation of the relative density of electrons, n_r , as a function of the applied field.

2.5 Bilayered memristive-like model

2.5.1 Electron conduction

To model our system, we consider two elements in parallel as illustrated in the schematic in Figure 6. The geometry of the bilayered network, in which the 30 nm thick ns-Au film is deposited below the 90 nm thick ns-ZrOx film, suggests such a parallel architecture. Furthermore, a similar parallel connection between two electrical components, representing a bulk and an interface

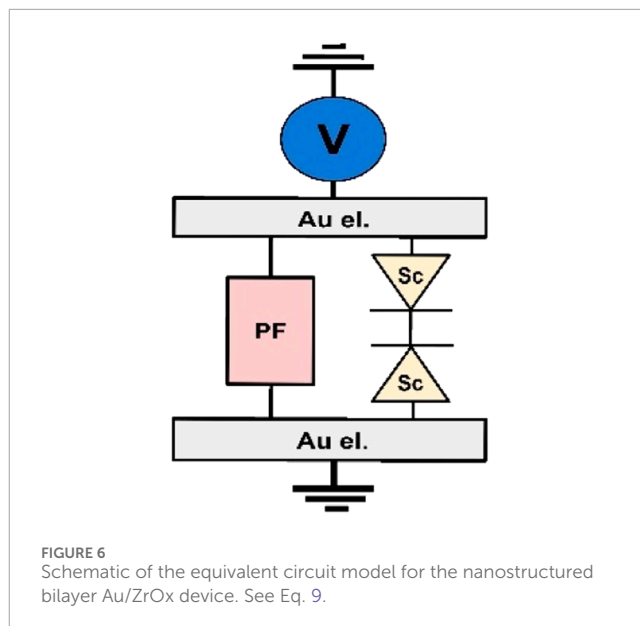


conduction mechanisms, is reported in literature for a Schottky in parallel with a SCLC mechanism in (Gomez-Marlasca et al., 2013) and in a simpler fashion by diodes in parallel and series with a interface and bulk resistances respectively in (Acha, 2011). Furthermore, the nanogranular structure of the film promotes local phenomena of ion migration and structural reorganization (Yun et al., 2016) providing a high network responsiveness to the formation of different conductive paths. We are here interested in developing an ideal model describing the main conduction mechanisms, the resistance of the electrodes is hence neglected but they can be implemented in the model with a resistance in series. The first element, depicted as a diode on each interface, as similarly reported in (Gomez-Marlasca et al., 2013) and in (Yang et al., 2008), refers to the electrode-limited conduction which is modelled as Schottky effect according to equation:

$$J_{Sc} = Ae^{\gamma\sqrt{E}} \quad (7)$$

where J_{Sc} is the current density and E is the externally applied field. A is a fitting parameter that takes care of the constant temperature of the device, the Richardson constant and the exponential prefactor with the Schottky barrier height. The parameter γ is another fitting constant which takes care of the electron charge and the dielectric constant of the amorphous material which is not easily accessible experimentally. Both zirconia and gold clusters interconnected networks can promote such an electrode-limited conduction, since cluster-assembled gold films show similar non-linear electrical behavior by themselves (Mirigliano et al., 2019; Nadalini et al., 2023).

The second element represents the PF effect for the bulk conduction. Similarly to what we propose, thin Ba_{0.8}Sr_{0.2}TiO₃/ZrO₂ heterostructures in a metal-insulator-metal (MIM) configuration resemble Schottky conduction at low electric fields and PF conduction at high ones, probably related to deep trap levels (Sahoo et al., 2013). These two conduction mechanisms have been proposed competing also in the conduction properties of a sputter-deposited Al/ZrO₂/Si structure (Chiu et al., 2005) and in the case of thin film metal-insulator-metal capacitors in a unified theory (Lau, 2012). Moreover, the nanostructured gold layer underneath



the ZrO_x layer enhances the effective field, leading to the saturation of the PF effect for larger voltages applied across the device.

According to this consideration, the standard PF of Eq. 3 is not sufficient to describe the conduction in our device, hence we use the PF equation as proposed by (Ongaro and Pillonnet, 1989). The current density flowing into this element is:

$$J_{PF} = q\mu N_c n_r E = B n_r E \quad (8)$$

where B is a fitting parameter that takes care of those physical parameters that are not easily accessible from an experimental point of view for an amorphous film as ours, i.e., the density of donor traps, N_c , the mobility of electrons in the low conduction band (or quasi-conduction band for amorphous films), μ . The relative density n_r , is modelled with Eq. 8 provided by (Ongaro and Pillonnet, 1989) and it incorporates the parameters η, z, c and s discussed in Section 2.4.

The total current density flowing into the device is ruled by the following equation:

$$J(v) = \begin{cases} wJ_{PF}(v) + (1-w)J_{Sc}(v), & \text{if } v > 0 \\ -((1-w)J_{PF}(|v|) + wJ_{Sc}(|v|)), & \text{if } v < 0 \end{cases} \quad (9)$$

where $w \in [0, 1]$ is the first order state variable that rules the relative contributions of the bulk-limited PF effect and the electrode-limited Schottky effect. The state variable dynamics describes the motion of ions through the device. The current densities are written as functions of the applied voltage, rather than functions of the field as in Eqs 7, 8.

A phenomenon introduced by such nanogranular systems is that grain boundaries and defects promote the formation of barrier layers (Whangbo and Subramanian, 2006; Felix et al., 2011), responsible for dielectric properties of the material which affect both γ and B already mentioned parameters, present in Schottky and Poole-Frenkel mechanisms respectively.

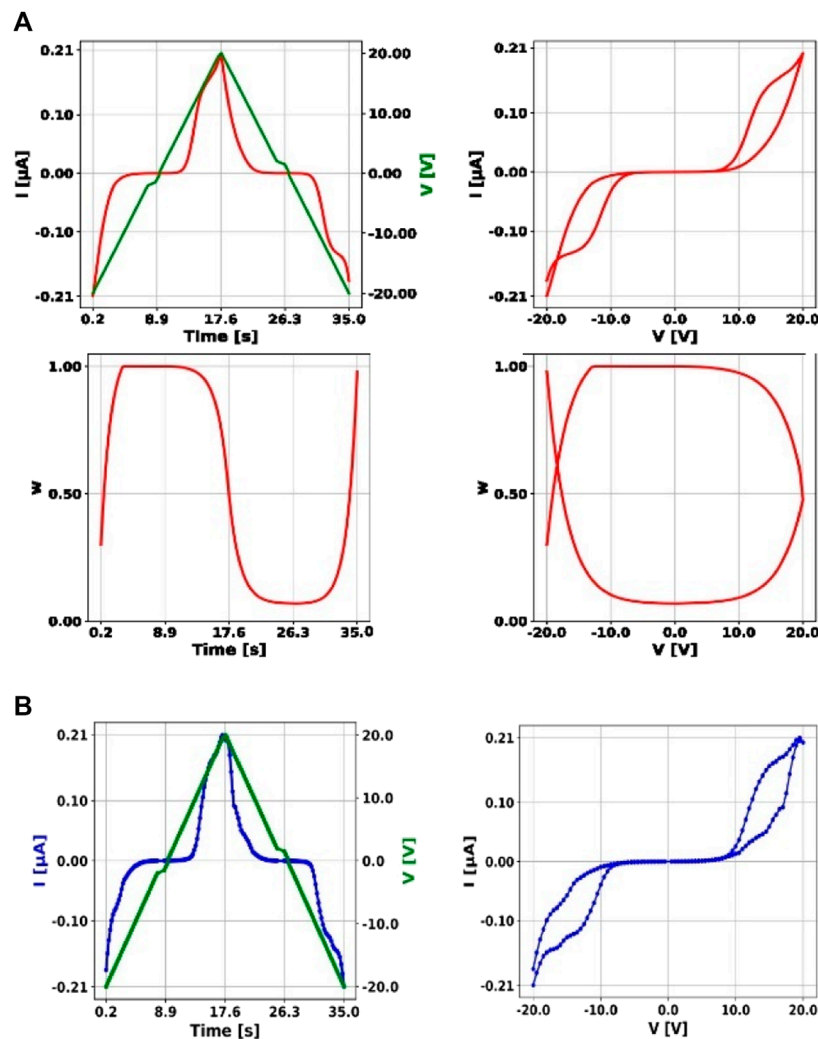


FIGURE 7

Comparison between our model and measured data. In (A) the simulation of an IV sweep at 2.3 V/s. In the first row, the current and the applied voltage as a function of time are depicted on the left, while on the right the I-V characteristics of the simulated device is shown. On the bottom row, the state-variable is plotted *versus* time (left) and *versus* the applied voltage (right). In (B) the experimental data are shown for comparison both in time (left) and in the I-V plane.

2.5.2 Ion migration

The application of a voltage difference between the electrodes results in the field-driven migration of the ions species through the insulating layer towards the cathode electrode. Ion species might consist of positive ones or oxygen vacancies in the ZrO_x layer as similarly reported for the case of (Gomez-Marlasca et al., 2013) and by first-principles calculations in (Shi et al., 2014) as well as metallic ions either injected in the device from the metallic electrodes or from the nanostructured surface of the gold layer below the zirconia layer. The presence of grain boundaries and defects in the nanostructured zirconia layer can favor ion mobility (Yun et al., 2016). Compared to devices made of thin-oxide-film sandwiched between two metals, in our device filament formation spanning the large device size is less likely. The slow ions motion, when compared to the (almost) instantaneous electronic motion, results in a redistribution of charge at the electrode interface which results in a modification of the Schottky barrier at the forced electrode (Yang et al., 2008; Acha,

2011; Gomez-Marlasca et al., 2013), and *vice versa* for negative applied voltage.

The motion of ions is modelled according to the *sinh-model* equation from (Chang et al., 2011):

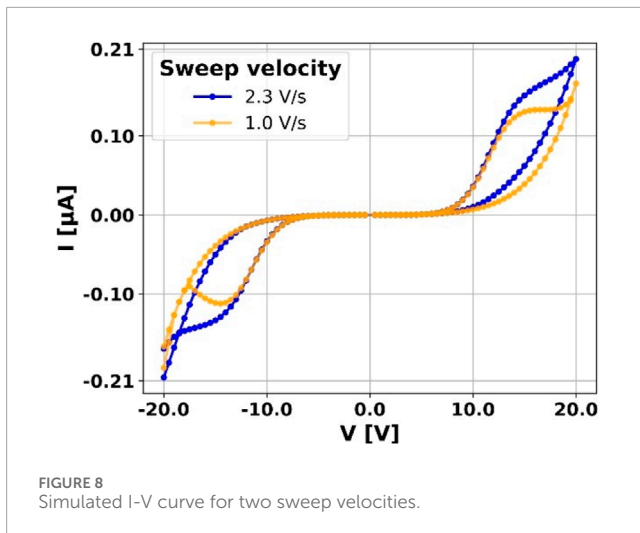
$$\frac{dw}{dt} = -\lambda \left(e^{\frac{v}{v_p}} - e^{-\frac{v}{v_n}} \right) \quad (10)$$

where λ is the drift velocity, v_n and v_p are activation thresholds.

3 Results and discussion

3.1 Validation of the bilayered model

To fit the parameters of our model, we used the experimental data shown in Figure 7B. Simulation results for a complete cycle, -20 to 20 V, are illustrated in Figure 7A. The relevant features of



the curves, such as the opening of the hysteresis for both non-zero voltages and currents and the saturation effect, are captured by our model. Figure 7 shows on top-left the current time evolution (red curve) for a triangular voltage signal (green curve) applied. The same dynamics is plotted in the I-V plane in the top-right of the figure. In the second row, the state variable w is plotted in time and against the applied voltage signal. In Figure 7B the experimental data are shown for comparison.

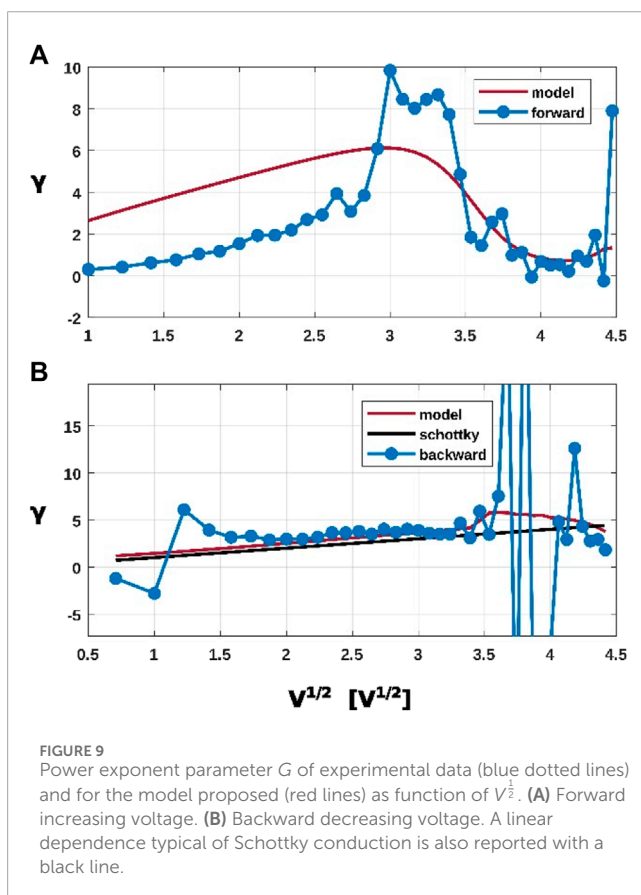


Figure 8 shows the simulated I-V curves for two voltage sweep velocities: 2.3 V/s (blue) and 1.0 V/s (orange). Simulation results are in good agreement with experimental measurements (see the experimental I-V characteristic shown in Figure 2) and (Profumo et al., 2023). Furthermore, a good agreement with parameters of (Chiu et al., 2005) is obtained. Fixing T at ambient temperature we obtained a $\Phi_p = 0.7$ V (1.1 V in (Chiu et al., 2005)) and, given a characteristic length over which the voltage is applied of 200 nm (which is reasonable due to the confinement effect of the Au clusters and corresponding to a medium electric field of 1 MV/cm), a $\epsilon_r = 6,5$ ($\epsilon_r = 6,25$ in (Chiu et al., 2005)). To obtain all curves shown in this section, an initial non-zero guess for the initial condition of the state variable was given as it is reasonable to assume that the initial DC bias of -20 V affects the initial state of the internal state variable.

Limitations of our modelling are believed to be due to the role of second order state variables, as the temperature. In fact, temperature affects both the mobility of ions and the electronic description, thus its role needs to be investigated for future modelling of this device. Furthermore, our modelling does not take into account spontaneous relaxation of the device.

3.2 Experimental IV curves at different temperatures

An analysis from experimental data of the power exponent parameter $G = d \ln(I) / d \ln(V)$ (Acha, 2017) at room temperature gives an insight into the different predominant conduction mechanisms in the two regimes of the hysteretic curve. In Figure 9 we report G curves as function of $V^{1/2}$ for the forward A) and backward B) branch of the positive voltage portion of the I-V curve, both for the experimental data (blue dots line) and the model proposed (red lines). The forward branch is well described by the model for high voltages while for low voltage a significant discrepancy arises. Furthermore, the peak in the forward gamma curve is often recognized in the case of PF conduction with a resistor in series and one in parallel (Acha, 2011; 2017; Acha et al., 2016). On the other hand, for the backward branch the model well describes the experimental curve besides for the raising of resistive switching activity (here clearly present in the raw data, note that some data points are out of the figure box). A zero-passing linear dependence (characteristic of pure Schottky interfaces) is also reported. These curves further support the hypothesis of the two mechanisms proposed in the memristive-like model. Nevertheless, they underline a poor accuracy of the model at low voltage which can be justified considering a higher noise in the experimental measurement at low voltages and due to capacitive effects (Zhou et al., 2020).

Remarkably, Poole-Frenkel (P-F) emission involves a process similar to Schottky emission, in which thermally excited electrons emit from traps into the dielectric's conduction band. P-F emission is thus also known as internal Schottky emission (Zafar et al., 1998) and no marked distinction can be made between the bulk- and electrode-limited conduction mechanisms (Chiu, 2014) especially in such a nanogranular structure (Felix et al., 2011). The slower dynamics of ionic migration (when compared to the electrons' almost-instantaneous dynamics) regulates the switching between

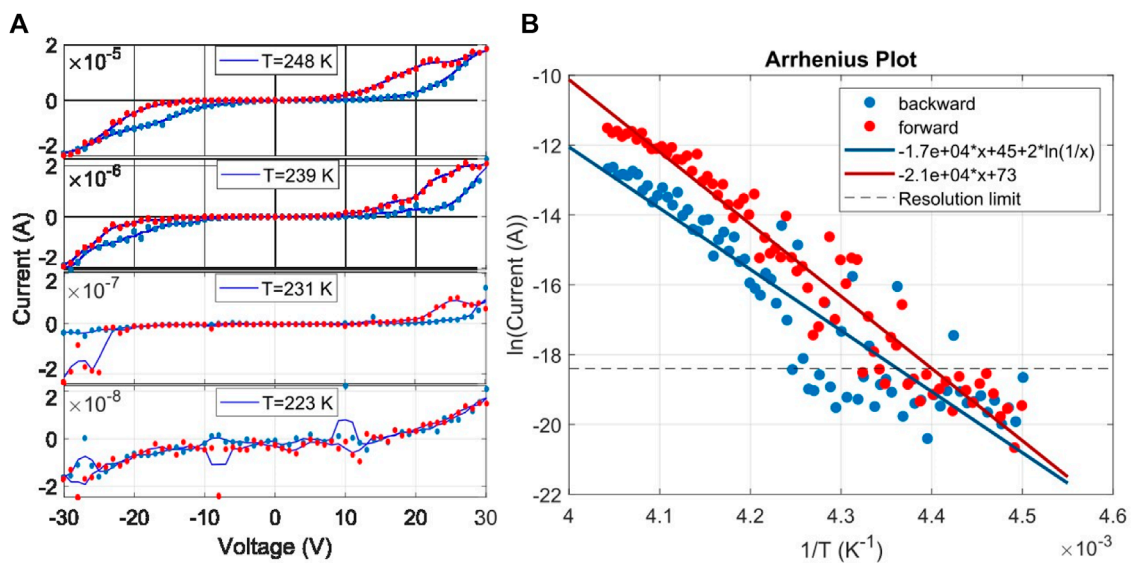


FIGURE 10

(A) DC I-V sweep for a layered Au/ZrO_x samples at different temperatures after resistive switching activation. A continuous line corresponds to a moving average with five points window. Legend shows the mean temperature of each sweep. (B) Arrhenius plot showing the evolution of current at +20 V for a layered Au/ZrO_x with the inverse of the temperature. The multimeter resolution limit is reported as a horizontal dashed line. Fit of these data, for forward and backward ramps, are carried out with the Poole-Frenkel and Schottky formula, which give the main contribution in each of these two ramps, respectively.

the two conduction mechanisms involved, particularly promoted by the network responsiveness.

The low sensitivity of the *in-situ* apparatus at low current values prevented us from the evaluation of the gamma parameter at lower temperatures. Nevertheless, we reported in Figure 10A representative IV curves acquired at three decreasing temperatures, and on the right (Figure 10B) the Arrhenius plot of the current at +20 V, for the backward and forward voltage ramps. These data confirm a hysteretic behavior of the current decreasing at lower temperatures. Furthermore, an exponential fit of the Arrhenius plot stress the accuracy of the proposed model, given the expected temperature dependence of both the Schottky and the Poole-Frenkel mechanisms. For the backward ramp where we propose a main contribute of the Schottky mechanism, a quadratic term in T is included (note that this term has not significant contribute to the fitted curve). The decrease of the hysteresis with temperature can be interpret also with the decreasing mobility of oxygen vacancies in the film (Aleskandrova et al., 2006).

4 Conclusion

A description of the conduction behavior of a nanostructured bilayer Au/ZrO_x film has been proposed as a result of the interplay of a PF and a Schottky mechanisms; on this base a memristive-like model for the devices has been developed. Our model accounts for the electrical hysteretic behavior observed in experimental set-up of a nanogranular network, where ion migration and network reorganization are well promoted. The model is based on ion migration which regulates the relative contribution of two mechanisms of electrical conduction proposed. Electrode-limited

conduction is modelled as Schottky effect, while bulk-limited conduction is modelled according to the Poole-Frenkel (PF) effect, where the presence of the two nanogranular materials, full of grain boundaries and defects, promote each of the two mechanisms. In this work we used a refined model for the PF effect which integrates the saturation at high field due to the complete ionization of the traps. Moreover, our model shows good agreement with the experimental data for multiple voltage sweep-velocity as for electrical measurement at different temperatures, as also with power exponent parameter curves.

Both LTSpice and Python code to simulate the memristor are provided (see Supplementary Material).

Data availability statement

The raw data supporting the conclusion of this article will be made available by the authors, without undue reservation.

Author contributions

DC: Writing—original draft, Writing—review and editing, Methodology. FP: Writing—review and editing, Investigation. LS: Writing—review and editing. PM: Writing—review and editing. FB: Writing—review and editing, Investigation.

Funding

The author(s) declare that financial support was received for the research, authorship, and/or publication of this article. This

work was partially funded by EUs Horizon 2020, from the MSCA-ITN-2019 Innovative Training Networks program “Materials for Neuromorphic Circuits” (MANIC) under the grant agreement No. 861153. Financial support by the Groningen Cognitive Systems and Materials Center (CogniGron) is gratefully acknowledged. (Corresponding author: DC).

Acknowledgments

We thank Andrea Falqui for the ESEM investigation of the nanostructured nanocomposite sample. We thank Francesco Cavaliere, Licia Pizzo, Giorgio Dall’Oglio and Lorenzo Martinis for providing and operating the cryogenic apparatus used for the low temperature measurements.

Conflict of interest

The authors declare that the research was conducted in the absence of any commercial or financial relationships

References

- Acha, C. (2011). Dynamical behaviour of the resistive switching in ceramic YBCO/metal interfaces. *J. Phys. D Appl. Phys.* 44 (34), 345301. doi:10.1088/0022-3727/44/34/345301
- Acha, C. (2017). Graphical analysis of current-voltage characteristics in memristive interfaces. *J. Appl. Phys.* 121 (13), 134502. doi:10.1063/1.4979723
- Acha, C., Schulman, A., Boudard, M., Daoudi, K., and Tsuchiya, T. (2016). Transport mechanism through metal-cobaltite interfaces. *Appl. Phys. Lett.* 109 (1), 011603. doi:10.1063/1.4955204
- Aleskandrova, P. V., Gueorguiev, V. K., Ivanov, Tz. E., and Koprinarova, J. B. (2006). Poole-Frenkel conduction in Al/ZrO₂/SiO₂/Si structures. *Eur. Phys. J. B - Condens. Matter Complex Syst.* 52 (4), 453–457. doi:10.1140/epjb/e2006-00335-2
- Borghini, F., Mirigliano, M., Dellasega, D., and Milani, P. (2022). Influence of the nanostructure on the electric transport properties of resistive switching cluster-assembled gold films. *Appl. Surf. Sci.* 582, 152485. doi:10.1016/j.apsusc.2022.152485
- Borghini, F., Podestà, A., Piazzoni, C., and Milani, P. (2018). Growth mechanism of cluster-assembled surfaces: from submonolayer to thin-film regime. *Phys. Rev. Appl.* 9 (4), 044016. doi:10.1103/PhysRevApplied.9.044016
- Bose, S. K., Mallinson, J. B., Gazoni, R. M., and Brown, S. A. (2017). Stable self-assembled atomic-switch networks for neuromorphic applications. *IEEE Trans. Electron Devices* 64 (12), 5194–5201. doi:10.1109/TED.2017.2766063
- Casu, A., Chiodoni, A., Ivanov, Y. P., Divitini, G., Milani, P., and Falqui, A. (2024). *In situ* TEM investigation of thermally induced modifications of cluster-assembled gold films undergoing resistive switching: implications for nanostructured neuromorphic devices. *ACS Appl. Nano Mater.* 7 (7), 7203–7212. doi:10.1021/acsnm.3c06261
- Chang, T., Jo, S.-H., Kim, K.-H., Sheridan, P., Gaba, S., and Lu, W. (2011). Synaptic behaviors and modeling of a metal oxide memristive device. *Appl. Phys. A* 102 (4), 857–863. doi:10.1007/s00339-011-6296-1
- Chiu, F.-C. (2014). A review on conduction mechanisms in dielectric films. *Adv. Mater. Sci. Eng.* 2014, 1–18. doi:10.1155/2014/578168
- Chiu, F.-C., Lin, Z.-H., Chang, C.-W., Wang, C.-C., Chuang, K.-F., Huang, C.-Y., et al. (2005). Electron conduction mechanism and band diagram of sputter-deposited Al/ZrO₂/Si structure. *J. Appl. Phys.* 97 (3), 034506. doi:10.1063/1.1846131
- Christensen, D. V., Dittmann, R., Linares-Barranco, B., Sebastian, A., Gallo, M. L., Redaelli, A., et al. (2022). 2022 roadmap on neuromorphic computing and engineering. *Neuromorphic Comput. Eng.* 2 (2), 022501. doi:10.1088/2634-4386/ac4a83
- Chua, L. O. (1971). “Memristor-The missing circuit element,” in *IEEE Transactions on Circuit Theory* 18 (5), 507–519. doi:10.1109/TCT.1971.1083337
- Chua, L. O., and Kang, S. M. (1976). Memristive devices and systems. *Proc. IEEE* 64 (2), 209–223. doi:10.1109/PROC.1976.10092

that could be construed as a potential conflict of interest.

Publisher’s note

All claims expressed in this article are solely those of the authors and do not necessarily represent those of their affiliated organizations, or those of the publisher, the editors and the reviewers. Any product that may be evaluated in this article, or claim that may be made by its manufacturer, is not guaranteed or endorsed by the publisher.

Supplementary material

The Supplementary Material for this article can be found online at: <https://www.frontiersin.org/articles/10.3389/fmats.2024.1385792/full#supplementary-material>

Cipollini, D., Swierstra, A., and Schomaker, L. (2024). Modeling a domain wall network in BiFeO₃ with stochastic geometry and entropy-based similarity measure. *Front. Mater.* 11. doi:10.3389/fmats.2024.1323153

Emelyanov, A. V., Nikiruy, K. E., Demin, V. A., Rylkov, V. V., Belov, A. I., Korolev, D. S., et al. (2019). Yttria-stabilized zirconia cross-point memristive devices for neuromorphic applications. *Microelectron. Eng.* 215, 110988. doi:10.1016/j.mee.2019.110988

Felix, A. A., Orlandi, M. O., and Varela, J. A. (2011). Schottky-type grain boundaries in CCTO ceramics. *Solid State Commun.* 151 (19), 1377–1381. doi:10.1016/j.ssc.2011.06.012

Filatov, D., Antonov, D., Antonov, I., Kasatkin, A., and Gorshkov, O. (2017). Resistive switching in stabilized zirconia films studied by conductive atomic Force microscopy. *J. Mater. Sci. Chem. Eng.* 05 (01), 8–14. doi:10.4236/msce.2017.51002

Filatov, D., Kazantseva, I., Antonov, D., Antonov, I., Shenina, M., Pavlov, D., et al. (2018). Conductive atomic Force microscopy study of the resistive switching in yttria-stabilized zirconia films with Au nanoparticles. *Scanning* 2018, 1–9. doi:10.1155/2018/5489596

Frenkel, J. (1938). On pre-breakdown phenomena in insulators and electronic semiconductors. *Phys. Rev.* 54 (8), 647–648. doi:10.1103/PhysRev.54.647

Fu, T., Liu, X., Gao, H., Ward, J. E., Liu, X., Yin, B., et al. (2020). Bioinspired bio-voltage memristors. *Nat. Commun.* 11 (1), 1861. Article 1. doi:10.1038/s41467-020-15759-y

Gomez-Marlasca, F., Ghenzi, N., Leyva, A. G., Albornoz, C., Rubi, D., Stoliar, P., et al. (2013). Modeling electronic transport mechanisms in metal-manganite memristive interfaces. *J. Appl. Phys.* 113 (14), 144510. doi:10.1063/1.4800887

Gorshkov, O. N., Mikhaylov, A. N., Kasatkin, A. P., Tikhov, S. V., Filatov, D. O., Pavlov, D. A., et al. (2016). Resistive switching in the Au/ZrO₂/Y₂O₃/TiN/Ti memristive devices deposited by magnetron sputtering. *J. Phys. Conf. Ser.* 741 (1), 012174. doi:10.1088/1742-6596/741/1/012174

Guseinov, D. v., Tetelbaum, D. i., Mikhaylov, A. n., Belov, A. i., Shenina, M. e., Korolev, D. s., et al. (2017). Filamentary model of bipolar resistive switching in capacitor-like memristive nanostructures on the basis of yttria-stabilised zirconia. *Int. J. Nanotechnol.* 14 (7–8), 604–617. doi:10.1504/IJNT.2017.083436

Harrell, W. R., and Gopalakrishnan, C. (2002). Implications of advanced modeling on the observation of Poole-Frenkel effect saturation. *Thin Solid Films* 405 (1–2), 205–217. doi:10.1016/S0040-6090(01)01752-7

Hill, R. M. (1971). Poole-Frenkel conduction in amorphous solids. *Philosophical Mag. A J. Theor. Exp. Appl. Phys.* 23 (181), 59–86. doi:10.1080/14786437108216365

Hinton, G. E., and Brown, A. D. (2000). “Spiking Boltzmann machines,” in *Advances in Neural Information Processing Systems*. Editors A. Solla, T. K. Leen, and K. R. Müller Vol. 12 (Cambridge: MIT Press), 122–128.

- Hopfield, J. J. (1982). Neural networks and physical systems with emergent collective computational abilities. *Proc. Natl. Acad. Sci. U. S. A.* 79 (8), 2554–2558. doi:10.1073/pnas.79.8.2554
- Indiveri, G., Linares-Barranco, B., Legenstein, R., Deligeorgis, G., and Prodromakis, T. (2013). Integration of nanoscale memristor synapses in neuromorphic computing architectures. *Nanotechnology* 24 (38), 384010. doi:10.1088/0957-4484/24/38/384010
- Jaeger, H. (2001) *The “echo state” approach to analysing and training recurrent neural networks—with an erratum note*. Bonn, Germany: German National Research Center for Information Technology GMD Technical Report, 148.
- Laiho, M., Lehtonen, E., Russell, A., and Dudek, P. (2010). Memristive synapses are becoming reality. Available at: <https://www.semanticscholar.org/paper/Memristive-synapses-are-becoming-reality-Laiho-Lehtonen/b8376c268ae11891d21a729778093dd77ab0953>.
- Lau, W. S. (2012). An extended unified Schottky-Poole-Frenkel theory to explain the current-voltage characteristics of thin film metal-insulator-metal capacitors with examples for various high-k dielectric materials. *ECS J. Solid State Sci. Technol.* 1 (6), N139–N148. doi:10.1149/2.006301jss
- Linn, E., Siemon, A., Waser, R., and Menzel, S. (2014). Applicability of well-established memristive models for simulations of resistive switching devices. *IEEE Trans. Circuits Syst. I Regul. Pap.* 61 (8), 2402–2410. doi:10.1109/TCSI.2014.2332261
- Liu, Z., Tang, J., Gao, B., Yao, P., Li, X., Liu, D., et al. (2020). Neural signal analysis with memristor arrays towards high-efficiency brain-machine interfaces. *Nat. Commun.* 11 (1), 4234. Article 1. doi:10.1038/s41467-020-18105-4
- Maass, W., Natschläger, T., and Markram, H. (2002). Real-time computing without stable states: a new framework for neural computation based on perturbations. *Neural Comput.* 14 (11), 2531–2560. doi:10.1162/089976602760407955
- Mead, C. (2020). How we created neuromorphic engineering. *Nat. Electron.* 3 (7), 434–435. Article 7. doi:10.1038/s41928-020-0448-2
- Milani, P., and Iannotta, S. (1999) *Cluster Beam synthesis of nanostructured materials*. Springer. doi:10.1007/978-3-642-59899-9
- Milano, G., Pedretti, G., Montano, K., Ricci, S., Hashemkhani, S., Boarino, L., et al. (2022). In materia reservoir computing with a fully memristive architecture based on self-organizing nanowire networks. *Nat. Mater.* 21 (2), 195–202. doi:10.1038/s41563-021-01099-9
- Mirigliano, M., Borghi, F., Podestà, A., Antidormi, A., Colombo, L., and Milani, P. (2019). Non-ohmic behavior and resistive switching of Au cluster-assembled films beyond the percolation threshold. *Nanoscale Adv.* 1 (8), 3119–3130. doi:10.1039/C9NA00256A
- Mirigliano, M., and Milani, P. (2021). Electrical conduction in nanogranular cluster-assembled metallic films. *Adv. Phys. X* 6 (1), 1908847. doi:10.1080/23746149.2021.1908847
- Nadalini, G., Borghi, F., Košutová, T., Falqui, A., Ludwig, N., and Milani, P. (2023). Engineering the structural and electrical interplay of nanostructured Au resistive switching networks by controlling the forming process. *Sci. Rep.* 13 (1), 19713. Article 1. doi:10.1038/s41598-023-46990-4
- Ongaro, R., and Pillonnet, A. (1989). Poole-Frenkel (PF) effect high field saturation. *Rev. Phys. Appliquée* 24 (12), 1085–1095. doi:10.1051/rphysap:0198900240120108500
- Parreira, P., Paterson, G. W., McVitie, S., and MacLaren, D. A. (2016). Stability, bistability and instability of amorphous ZrO₂ resistive memory devices. *J. Phys. D Appl. Phys.* 49 (9), 095111. doi:10.1088/0022-3727/49/9/095111
- Pickett, M. D., Strukov, D. B., Borghetti, J. L., Yang, J. J., Snider, G. S., Stewart, D. R., et al. (2009). Switching dynamics in titanium dioxide memristive devices. *J. Appl. Phys.* 106 (7), 074508. doi:10.1063/1.3236506
- Previdi, A., Borghi, F., Profumo, F., Schulte, C., Piazzoni, C., Lamanna, J., et al. (2023). Nanotopography and microconfinement impact on primary hippocampal astrocyte morphology, cytoskeleton and spontaneous calcium wave signalling. *Cells* 12 (2), 293. doi:10.3390/cells12020293
- Profumo, F., Borghi, F., Falqui, A., and Milani, P. (2023). Potentiation and depression behaviour in a two-terminal memristor based on nanostructured bilayer ZrO_x/Au films. *J. Phys. D: Appl. Phys.* 56 (35), 355301. doi:10.1088/1361-6463/acd704
- Rieck, J. L., Cipollini, D., Salverda, M., Quinteros, C. P., Schomaker, L. R. B., and Noheda, B. (2023). Ferroelastic domain walls in BiFeO₃ as memristive networks. *Adv. Intell. Syst.* 5 (1), 2200292. doi:10.1002/aisy.202200292
- Ryabova, M. A., Filatov, D. O., Shenina, M. E., Koryazhkina, M. N., Antonov, I. N., Baranova, V. N., et al. (2022). Resonant activation of resistance switching in memristors based on YSZ films with Au nanoparticles. *J. Phys. Conf. Ser.* 2227 (1), 012020. doi:10.1088/1742-6596/2227/1/012020
- Sahoo, S. K., Bakhru, H., Kumar, S., Misra, D., Wolden, C. A., Mohapatra, Y. N., et al. (2013). Field dependent carrier transport mechanisms in metal-insulator-metal devices with Ba_{0.8}Sr_{0.2}TiO₃/ZrO₂ heterostructured thin films as the dielectric. *MRS Online Proc. Libr.* 1547 (1), 53–60. doi:10.1557/opl.2013.855
- Schulte, C., Lamanna, J., Moro, A. S., Piazzoni, C., Borghi, F., Chighizola, M., et al. (2018). Neuronal cells confinement by micropatterned cluster-assembled dots with mechanotransductive nanotopography. *ACS Biomaterials Sci. Eng.* 4 (12), 4062–4075. doi:10.1021/acsbiomaterials.8b00916
- Schulte, C., Rodighiero, S., Cappelluti, M. A., Puricelli, L., Maffioli, E., Borghi, F., et al. (2016). Conversion of nanoscale topographical information of cluster-assembled zirconia surfaces into mechanotransductive events promotes neuronal differentiation. *J. Nanobiotechnology* 14 (1), 18. doi:10.1186/s12951-016-0171-3
- Shi, L. B., Wang, Y. P., and Li, M. B. (2014). Native defect formation and migration in monoclinic zirconium dioxide. *Mater. Sci. Semicond. Process.* 27, 586–592. doi:10.1016/j.mssp.2014.07.040
- Strukov, D. B., Snider, G. S., Stewart, D. R., and Williams, R. S. (2008). The missing memristor found. *Nature* 453 (7191), 80–83. Article 7191. doi:10.1038/nature06932
- Sun, B., Liu, Y. X., Liu, L. F., Xu, N., Wang, Y., Liu, X. Y., et al. (2009). Highly uniform resistive switching characteristics of TiN/ZrO₂/Pt memory devices. *J. Appl. Phys.* 5. doi:10.1063/1.3055414
- Tikhov, S., Gorshkov, O., Antonov, I., Morozov, A., Koryazhkina, M., and Filatov, D. (2018). Ion migration polarization in the yttria stabilized zirconia based metal-oxide-metal and metal-oxide-semiconductor stacks for resistive memory. *Adv. Condens. Matter Phys.* 2018, e2028491–e2028498. doi:10.1155/2018/2028491
- Wang, Z., Li, C., Song, W., Rao, M., Belkin, D., Li, Y., et al. (2019). Reinforcement learning with analogue memristor arrays. *Nat. Electron.* 2 (3), 115–124. Article 3. doi:10.1038/s41928-019-0221-6
- Wegner, K., Piseri, P., Tafreshi, H. V., and Milani, P. (2006). Cluster beam deposition: a tool for nanoscale science and technology. *J. Phys. D Appl. Phys.* 39 (22), R439–R459. doi:10.1088/0022-3727/39/22/R02
- Whangbo, M.-H., and Subramanian, M. A. (2006). Structural model of planar defects in CaCu₃Ti₄O₁₂ exhibiting a giant dielectric constant. *Chem. Mater.* 18 (14), 3257–3260. doi:10.1021/cm060323f
- Xia, Q., and Yang, J. J. (2019). Memristive crossbar arrays for brain-inspired computing. *Nat. Mater.* 18 (4), 309–323. Article 4. doi:10.1038/s41563-019-0291-x
- Yakopcic, C., Taha, T. M., Subramanyam, G., and Pino, R. E. (2013). Generalized memristive device SPICE model and its application in circuit design. *IEEE Trans. Computer-Aided Des. Integr. Circuits Syst.* 32 (8), 1201–1214. doi:10.1109/TCAD.2013.2252057
- Yang, J. J., Pickett, M. D., Li, X., Ohlberg, D. A. A., Stewart, D. R., and Williams, R. S. (2008). Memristive switching mechanism for metal/oxide/metal nanodevices. *Nat. Nanotechnol.* 3 (7), 429–433. Article 7. doi:10.1038/nnano.2008.160
- Yun, J. S., Seidel, J., Kim, J., Soufiani, A. M., Huang, S., Lau, J., et al. (2016). Critical role of grain boundaries for ion migration in formamidinium and methylammonium lead halide perovskite solar cells. *Adv. Energy Mater.* 6 (13), 1600330. doi:10.1002/aenm.201600330
- Zafar, S., Jones, R. E., Jiang, B., White, B., Kaushik, V., and Gillespie, S. (1998). The electronic conduction mechanism in barium strontium titanate thin films. *Appl. Phys. Lett.* 73 (24), 3533–3535. doi:10.1063/1.122827
- Zhou, G., Ren, Z., Sun, B., Wu, J., Zou, Z., Zheng, S., et al. (2020). Capacitive effect: an original of the resistive switching memory. *Nano Energy* 68, 104386. doi:10.1016/j.nanoen.2019.104386
- Zhu, R., Hochstetter, J., Loeffler, A., Diaz-Alvarez, A., Nakayama, T., Lizier, J. T., et al. (2021). Information dynamics in neuromorphic nanowire networks. *Sci. Rep.* 11 (1), 13047. Article 1. doi:10.1038/s41598-021-92170-7